

Local probing of Bloch mode dispersion in a photonic crystal waveguide

Rob J.P. Engelen¹, Tim J. Karle², Henkjan Gersen^{1,3},
Jeroen P. Korterik¹, Thomas F. Krauss², Laurens Kuipers^{1,4} and
Niek F. van Hulst¹

¹*Applied Optics Group, Department of Science & Technology and MESA⁺ Institute for Nanotechnology, University of Twente, P.O. Box 217, 7500 AE Enschede, The Netherlands*

²*Ultrafast Photonics Collaboration, School of Physics and Astronomy, University of St. Andrews, St. Andrews, Fife, KY16 9SS, United Kingdom*

³*current address: Center for Atomic-Scale Materials Physics (CAMP), University of Aarhus, DK-8000 Aarhus C, Denmark*

⁴*FOM Institute for Atomic and Molecular Physics (AMOLF), Kruislaan 407, 1098 SJ Amsterdam, The Netherlands*

engelen@amolf.nl

Abstract: The local dispersion relation of a photonic crystal waveguide is directly determined by phase-sensitive near-field microscopy. We readily demonstrate the propagation of Bloch waves by probing the band diagram also beyond the first Brillouin zone. Both TE and TM polarized modes were distinguished in the experimental band diagram. Only the TE polarized defect mode has a distinctive Bloch wave character. The anomalous dispersion of this defect guided mode is demonstrated by local measurements of the group velocity. The measured dispersion relation and measured group velocities are both in good agreement with theoretical calculations.

© 2005 Optical Society of America

OCIS codes: (120.5050) Phase measurement; (180.5810) Scanning microscopy; (230.7370) Waveguides; (260.2030) Dispersion

References and links

1. J.D. Joannopoulos, R.D. Meade, J.N. Winn, *Photonic Crystals: Molding the Flow of Light* (Princeton University Press, Princeton, NY, 1995)
2. See for example, *Photonic Crystals and Light Localization in the 21st Century*, in *NATO Science Series*, C.M. Soukoulis, ed. (Kluwer Academic, Dordrecht, The Netherlands, 2001)
3. H. Benisty, "Modal analysis of optical guides with two-dimensional photonic band-gap boundaries," *J. Appl. Phys.* **79** 7483–7492 (1996)
4. S.G. Johnson, P.R. Villeneuve, S. Fan, J.D. Joannopoulos, "Linear waveguides in photonic crystal slabs," *Phys. Rev. B* **62** 8212–8222 (2000)
5. X. Letartre, C. Seassal, C. Grillet, P. Rojo-Romeo, P. Viktorovitch, M.L. d'Yerville, D. Cassagne, C. Jouanin, "Group velocity and propagation losses measurement in a single-line photonic-crystal waveguide on InP membranes" *Appl. Phys. Lett.* **79** 2312–2314 (2001)
6. S. Olivier, H. Benisty, C.J.M. Smith, M. Rattier, C. Weisbuch, T.F. Krauss, "Transmission properties of two-dimensional photonic crystal channel waveguides," *Opt. Quantum Electron.* **34** 171–181 (2002)
7. K. Inoue, N. Kawai, Y. Sugimoto, N. Ikeda, K. Asakawa, "Observation of small group velocity in two-dimensional AlGaAs-based photonic crystal slabs," *Phys. Rev. B* **65** 121308 (2002)
8. T. Asano, K. Kiyota, D. Kumamoto, B.S. Song, S. Noda, "Time-domain measurement of picosecond light-pulse propagation in a two-dimensional photonic crystal-slab waveguide," *Appl. Phys. Lett.* **84** 4690–4692 (2004)
9. D. Mori, T. Baba, "Dispersion-controlled optical group delay device by chirped photonic crystal waveguides," *Appl. Phys. Lett.* **85** 1101–1103 (2004)
10. A.Y. Petrov, M. Eich, "Zero dispersion at small group velocities in photonic crystal waveguides" *Appl. Phys. Lett.* **85** 4866–4868 (2004)

11. P.St.J. Russell, "Bloch wave analysis of dispersion and pulse propagation in pure distributed feedback structures," *J. Mod. Opt.* **38** 1599–1619 (1991)
12. M. Lončar, D. Nedeljković, T.P. Pearsall, J. Vučković, A. Scherer, S. Kuchinsky, D.C. Allan, "Experimental and theoretical confirmation of Bloch-mode light propagation in planar photonic crystal waveguides," *Appl. Phys. Lett.* **80** 1689–1691 (2002)
13. P.E. Barclay, K. Srinivasan, M. Borselli, O. Painter, "Probing the dispersive and spatial properties of photonic crystal waveguides via highly efficient coupling from fiber tapers," *Appl. Phys. Lett.* **85** 4–6 (2004)
14. S.I. Bozhevolnyi, V.S. Volkov, T. Sondergaard, A. Boltasseva, P.I. Borel, M. Kristensen, "Near-field imaging of light propagation in photonic crystal waveguides: Explicit role of Bloch harmonics," *Phys. Rev. B* **66** 235204 (2002)
15. H. Gersen, T.J. Karle, R.J.P. Engelen, W. Bogaerts, J.P. Korterik, N.F. van Hulst, T.F. Krauss, L. Kuipers, "Direct observation of Bloch harmonics and negative phase velocity in photonic crystal waveguides," *Phys. Rev. Lett.* **94** 123901 (2005)
16. L. Vogelaar, W. Nijdam, H.A.G.M. van Wolferen, R.M. de Ridder, F.B. Segerink, E. Flück, L. Kuipers, N.F. van Hulst, "Large Area Photonic Crystal Slabs for Visible Light with Waveguiding Defect Structures: Fabricated with Focussed Ion Beam Assisted Laser Interference Lithography" *Adv. Mater.* **13** 1551–1554 (2001)
17. M.L.M. Balistreri, J.P. Korterik, L. Kuipers, N.F. van Hulst, "Phase mapping of optical fields in integrated optical waveguide structures," *J. Lightwave Technol.* **19** 1169–1176 (2001)
18. M.L.M. Balistreri, H. Gersen, J.P. Korterik, L. Kuipers, N.F. van Hulst, "Tracking femtosecond laser pulses in space and time," *Science* **294** 1080–1082 (2001)
19. H. Gersen, J.P. Korterik, N.F. van Hulst, L. Kuipers, "Tracking ultrashort pulses through dispersive media: Experiment and theory" *Phys. Rev. E* **68** 026604 (2003)
20. H. Gersen, T.J. Karle, R.J.P. Engelen, W. Bogaerts, J.P. Korterik, N.F. van Hulst, T.F. Krauss, L. Kuipers, "Real space observation of ultraslow light in photonic crystal waveguides," *Phys. Rev. Lett.* **94** 073903 (2005)
21. M.L.M. Balistreri, A. Driessen, J.P. Korterik, L. Kuipers, N.F. van Hulst, "Quasi interference of perpendicularly polarized guided modes observed with a photon scanning tunneling microscope," *Opt. Lett.* **25** 637–639 (2000)
22. G.P. Agrawal, *Nonlinear Fiber Optics* (Academic Press, San Diego, Calif., 2001)

1. Introduction

Photonic crystals [1] (PhCs) exhibit the unique potential to manipulate the flow of light at the wavelength scale and ultimately fabricate highly integrated optical devices [2]. PhCs consist of periodic arrangements of dielectric materials. With the proper geometric and material properties, a range of optical frequencies is forbidden to propagate for all possible crystallographic directions: a photonic bandgap. By selectively changing the local geometry of the PhC, localized states can be created. Specifically, an ordered series of defects can act as a waveguide for light, at otherwise forbidden frequencies [3, 4]. In practice, photonic crystal waveguides (PhCWs) are generally created in planar structures, where one is able to tailor the dispersion relation and hence properties like group velocity and transmission and reflection spectra [5, 6, 7, 8, 9, 10].

In a PhCW, the propagation of light is governed by Bloch's theorem due to the interplay between the light and the surrounding periodic structure [11]. Experimentally, this Bloch wave character of a PhCW mode has been deduced by detecting the out-of-plane leakage of light [12]. Using far-field input-output methods also modified transmission characteristics, pulse dispersion, and group-velocity alteration have been studied [7, 8]. However, an important drawback of these approaches is that the PhCW dispersion relation is averaged throughout the full length of the PhCW. As a result, any local information on the non-radiative modes within the PhCW is lost in input-output methods. The full picture can only be acquired by probing locally along the PhCW. Indeed recently, PhCW dispersion has been addressed by local evanescent field probing. This was demonstrated by either investigating the evanescent field coupling between a tapered optical fiber and a PhCW [13] or by local near-field probing of the intensity distribution in a PhCW [14]. Unfortunately, in both cases only a small portion of the total band diagram was obtained.

Here we present the full band structure of a PhCW by employing a truly field sensitive near-field optical microscope. By probing both the local phase and amplitude of the light propagating, the full range of wavevectors in the PhCW can be uncovered [15]. The dispersion

relation of the PhCW is experimentally determined and allows the various modes to be discriminated by their propagation mode. The propagation of light through a single-line defect is studied. This simple geometry allows an accurate comparison between theory and experiment. Moreover, the frequency dependence of the group velocity (group velocity dispersion) of the bandgap guided mode is investigated, demonstrating the anomalous dispersion of the photonic crystal waveguide mode.

2. Photonic crystal and near-field experiment

The photonic crystal waveguide consists of a silicon nitride membrane containing a hexagonal lattice of air holes. One row of holes is not perforated in the close-packed crystal direction ($\Gamma-K$). This specific linear arrangement of defects is commonly referred to as a W1 waveguide. Fabrication details can be found elsewhere [16]. The resulting structure is an air-bridge photonic crystal slab of silicon-rich nitride ($n=2.16$) of 160 nm thickness, 293 nm lattice periodicity (a) and a hole radius of 100 nm ($0.34a$).

The geometric parameters of the PhCW have been determined experimentally and are used to calculate the photonic band diagram of the PhCW. The results of a 3D FDTD simulation are presented in Fig. 1, for TE and TM polarized modes. In the crystal region, a PhC bandgap opens up in the visible spectrum for TE polarization (E-field in the plane of the crystal). Within the TE bandgap ($\lambda = 575 - 690$ nm) two defect modes are allowed to propagate. For the TM-polarization, no bandgap exists and light can only be confined to the waveguide by refractive index contrast, both in-plane and out-of-plane. By selecting only the modes with a high quality factor from the FDTD simulation, two TM modes are found. Both modes show good correspondence to a ridge-waveguide approximation, where one mode is confined to the waveguide and

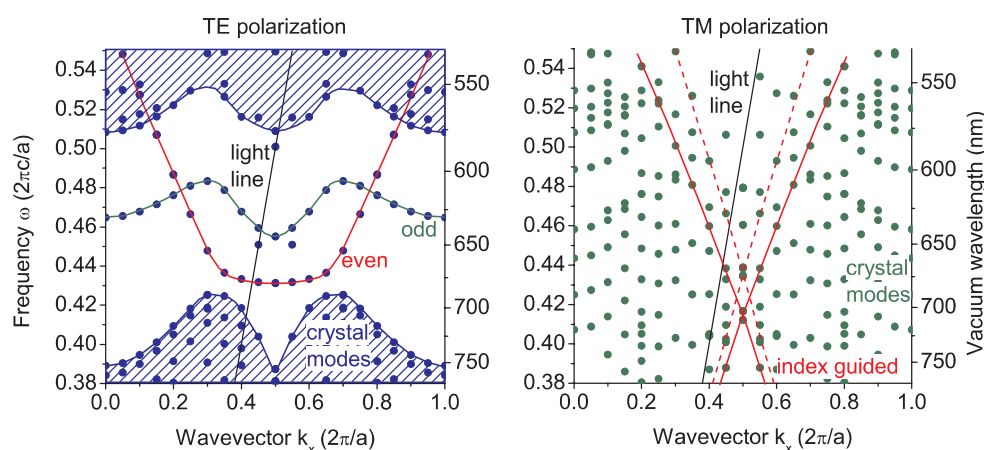


Fig. 1. Calculation of the dispersion relation of the W1 waveguide by 3D FDTD simulation for both TE (a) and TM polarization (b). In both figures, the solid dots represent the simulation results. (a) For TE polarization, the continuous curves represent the suggested dispersive modes. In the TE crystal bandgap, between $\omega=0.425$ and 0.510 (575-690nm), two modes are allowed to propagate. They are denoted even and odd by their in-plane symmetry. The shaded region depicts the crystal modes. (b) For TM polarization, the band diagram is dominated by crystal modes. The index guided waveguide mode and dominant crystal slab mode are drawn in red (solid and dashed lines, respectively). These bands are identified by mode solving and correspond to the modes with the lowest temporal decay in the FDTD simulation.

the other mode propagates within the slab. Therefore we assign the suggested modes to purely index-guided modes. These index-guided modes are highlighted by the red lines in Fig 1(b). However, for PhCW modes, it is probable that mini-stopgaps exist. These avoided crossings can in principle not be observed in the ridge-waveguide approximation.

Femtosecond laser pulses (250 ± 50 fs, near-Fourier limited) are provided by a frequency doubled Ti:Sapphire laser pumped optical parametric oscillator. This versatile laser system with tunability from 597 up to 675 nm enables a large part of the bandgap to be investigated. The laser light was coupled into the W1 waveguide by a 0.4 NA objective. In order to obtain the complete band diagram in the first experiment, both TE and TM polarized light were coupled in. For the measurements on group velocity dispersion, the TE polarization is selected.

In our near-field experiments an aluminum-coated fiber probe with a sub-wavelength aperture of approximately 90 nm is used to pick up the light from the structure. The optical field is recorded while scanning over the sample. The fiber probe is kept in close proximity (2-20 nm) to the PhCW surface by a shear-force feedback mechanism based on a tuning fork sensor. In this proximity region, the local evanescent field tail of the light propagating in the photonic structure is coupled to the probe. The collected light is mixed with a reference beam in a heterodyne interferometric arrangement. This way, the interference between the two branches is obtained, which allows both phase (ϕ) and amplitude (A) to be determined [17]. As raw data, the optical measurement yields the spatial distribution of $A \cos \phi$ and $A \sin \phi$. From these two parts of the raw data, the spatial amplitude distribution is calculated.

Also for a pulsed source we obtain the interference of the pulses, provided the collected and reference pulse overlap in time when they are mixed. In previous work [18, 19, 20], the arrival time of the reference pulse is fixed, i.e. the length of the reference branch is fixed while scanning an image. Thus a scan results in the spatial distribution of the interference. By varying the length of the reference branch between images, we can control the position of the interference maximum and thus track the femtosecond pulse through the PhCW.

3. Band diagram

In Fig. 2, the results of a near-field measurement at $\lambda=674$ nm ($\omega=0.435$) is depicted together with the corresponding electron micrograph of the PhC structure as a reference. The propagation of light within the PhCW is clearly visible in the field amplitude distribution as a bright horizontal line in Fig 2(c). On close examination of the optical field in the waveguide, the lattice periodicity can be recognized in the amplitude distribution. Another striking feature is the field

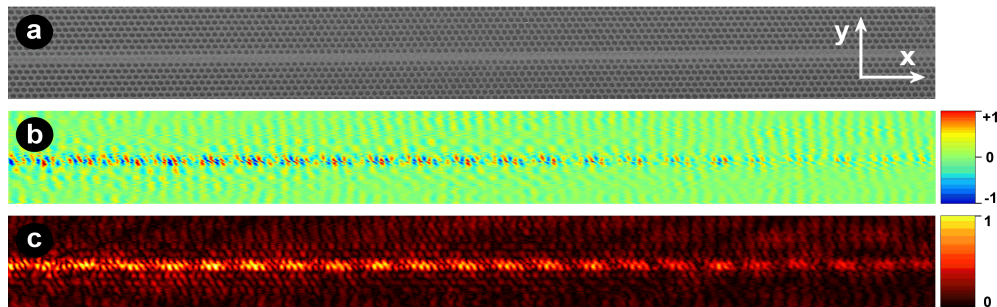


Fig. 2. Image sizes: $41 \mu\text{m} \times 4 \mu\text{m}$ (a) SEM image of the W1 waveguide under investigation. (b,c) Result of a near-field measurement on a PhCW with $\lambda = 674$ nm. (b) Measured distribution of $A \cos \phi$. (c) Normalized distribution of the amplitude of the evanescent optical field.

amplitude modulation along the waveguide with a period of approximately 6 lattice spacings. The beat pattern indicates the presence of multiple modes in the waveguide. Note that due to the simultaneous detection of TE and TM polarized light, quasi-interference can be observed in the measurements between perpendicular polarizations [21]. Therefore, the amplitude modulations are not necessarily caused by modes of equal polarization.

Each mode has a different phase velocity with a corresponding periodicity of phase fringes and spatial wavevector. From the combined amplitude ($A(x,y)$) and phase ($\phi(x,y)$) information ($A \cos \phi$) in Fig. 2(b), the contributing wavevectors are directly recovered by examining the spatial frequencies along the waveguide [17].

The retrieved optical data contain both $A \cdot \cos(\phi)$ and $A \cdot \sin(\phi)$ and thus describe the full complex field $A \cdot \exp(i\phi)$ in the structure. A complex Spatial Fourier Transformation (SFT) of the measured field is performed in order to retrieve both the wavevector (k_x) and amplitude (A) of the field propagating. The SFT of the complex optical field also reveals the sign of k_x , i.e. both positive and negative wavevectors. This approach provides more insight in the wavevector spectrum compared to our previous work [15, 17], where the real part of the field was Fourier transformed, projecting all k_x values on the positive axis.

The Fourier transforms are calculated for all horizontal lines in the scanned area (x-direction in Fig. 2,) and subsequently summed to retrieve the SFT representing the full measurement at a single optical frequency. A series of SFT results is depicted in Fig. 3 for measurements in the vacuum wavelength range from 597 nm ($\omega = 0.491$) up to 675 nm ($\omega = 0.434$). Each SFT is drawn in a false-color representation at its corresponding optical frequency. In this way, the spatial Fourier components are shown both as a function of the spatial frequency (k) and the temporal frequency (ω), resulting in the band diagram of the PhCW [15].

Several separate dispersion curves are visible in Fig. 3. By comparing the experimental band diagram to the calculated diagram of Fig. 1, we can assign a propagation mode to each dispersion curve. The curve denoted “Air” in Fig. 3 corresponds simply to the theoretical light line ($\omega = ck_x$). The curve is therefore the result of light skimming the surface, but still travelling through the air.

The results of the 3D FDTD simulation and the suggested dispersion curves are also shown in Fig. 3. For clarity, the simulation points for TM polarization are not shown. The measured band diagram matches the simulation results very well. In order to achieve good overlap between simulation and experiment, the FDTD results for TE polarization are plotted at 97% of their original frequency. This minor difference between experiment and simulation can be attributed to small deviations in the measurement of the geometrical parameters of the PhC structure.

The most striking feature in the measured dispersion relation are the positions of the curves which are assigned to a mode with TE polarization. An exact copy of this dispersion curve is present in both the negative and positive part of the band diagram. Because the waveguide is embedded in a photonic crystal, the propagating light experiences a periodic modulation of the dielectric constant. Therefore, the light must obey Bloch’s theorem. Hence, a waveguide mode is composed of multiple wavevectors, spaced $2\pi/a$ apart in reciprocal space. A fundamental mode with wavevector k_x has higher and lower harmonics at $k_x + n(2\pi/a)$, where $n \in \mathbb{Z}$. All together these harmonics form a single Bloch mode [11, 15]. Multiple harmonics in a structure together lead to a periodic amplitude modulation that coincides exactly with the periodic modulation of the dielectric constant (a). In our experiment, the even TE mode is found at spatial frequencies k_x and $k_x - 2\pi/a$. Hence, we have direct proof of the Bloch-wave light propagation in PhCWs.

Also the odd-symmetric TE mode can be recognized in the experimental dispersion relation. This mode is found at frequencies ~ 0.005 lower than the simulated band. The odd mode is particularly strong around $\omega=0.45$ and can be seen clearly around the wavevectors -0.4 and 0.6 .

Note also the very strong Bloch wave character, attributed to the strong harmonic with negative wavevector.

In addition to the TE modes in the bandgap, we also observe two index guided TM modes, denoted “TM” in Fig. 3. It is remarkable that, these modes have a much weaker component in the negative k -region. Since the TM modes propagate through the same structure, they also experience the periodic structure of the photonic crystal, and one would expect a Bloch-mode character also for index-guided TM modes. In Fig. 3, we clearly see that the even TE mode has a much stronger Bloch harmonic in the negative part of the dispersion relation compared to the TM modes. Apparently, the effective index modulation experienced by the TM modes is much lower compared to the TE mode, resulting in considerably stronger Bloch harmonics for TE polarization [11]. Therefore, we conclude that index guiding is dominant for the propagation of the TM modes.

By Fourier filtering we found that one TM propagation mode is localized in the defect area, like a waveguide mode, whereas the other resides in the crystal region. Due to the complex TM band structure (Fig. 1(b)), it is difficult to assign a specific TM crystal mode. Still, the found mode shows good correspondence to planar waveguiding, with an average refractive index of 42% air ($n=1$) and 58% silicon-rich nitride ($n=2.16$). Remarkably, the TM polarized light

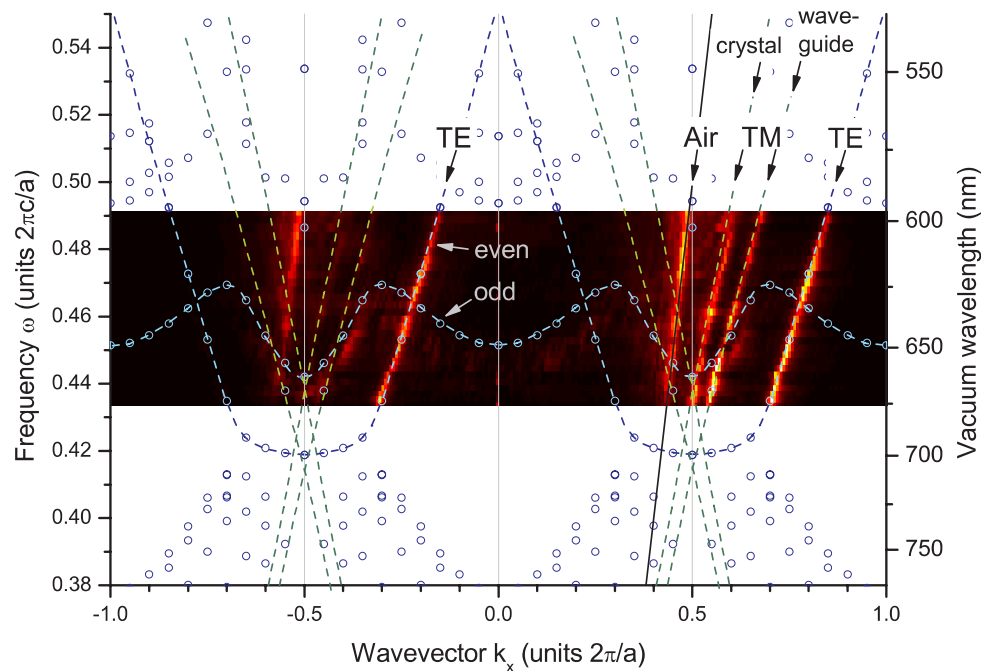


Fig. 3. Measured photonic band diagram of the W1 PhCW. Spatial Fourier Transforms (SFTs) of the measured $A \cos \phi$ of the optical field along the waveguide direction. The SFTs are represented by a linear false-color scale at their corresponding optical frequencies. Peaks represent the resonant wavevectors in the waveguide. The calculated dispersion relations of the TE modes are plotted in blue. The even and odd waveguide modes (TE polarization) are represented by the dashed blue lines. The index guided TM modes (waveguide and crystal) are both indicated by dashed green lines. Finally the light line ($\omega = ck_x$) is drawn in solid black.

couples preferentially to index guided modes, which we attribute to a large overlap between the mode symmetry of the index guided modes and the incoming plane wave.

Note the apparent Bloch character of the air-guided light. A copy of the light line is present at $\omega = c(k_x - 2\pi/a)$. This is a measurement artefact. Since the air guided light skims over the sample surface, it scatters at the lattice sites. This spatial periodic scattering causes an artificial amplitude modulation, similar to what is observed for Bloch waves. This measurement artefact causes the copy of the light line at $\omega = c(k_x - 2\pi/a)$. In contrast to this, the Bloch harmonics for the TE and TM modes are not an artefact as here the SFT along the waveguide line still shows the harmonics, while the scattering loss is negligible. In ref. [15], the spatial distribution of Bloch harmonics is investigated in greater detail.

Interestingly, the simulation shows a dramatically reduced group velocity for the even TE-polarized waveguide mode at the zone edge, around a vacuum wavelength of 700 nm ($\omega = 0.42$). Unfortunately, our laser system was not tunable beyond 675 nm. Therefore, the corresponding flattening of the photonic band could not be observed in the measured dispersion relation (Fig. 3). However, with a direct measurement of the group velocity, the initial group velocity reduction due to the band flattening can be investigated, since the group velocity determines the slope of the dispersion curve.

4. Probing the group velocity dispersion

To this end we exploit the femtosecond pulses in our near-field experiment to retrieve the group velocity of the light propagating. In our heterodyne set-up we obtain the interference of the pulse travelling through the PhCW (signal) and a reference pulse travelling through the air. In contrast to the previous experiment, we keep the fiber probe at a fixed position on the waveguide and vary the length of the reference branch. Thus we obtain a field cross-correlation function of the two pulses in time instead of space. The arrival time of the signal pulse can be determined directly by measuring the position of the maximum of the interference envelope. We repeat the experiment at different sample positions, for which the pulse arrival time will be different.

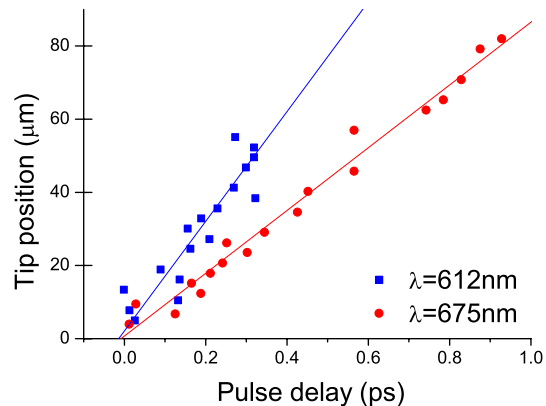


Fig. 4. Group velocity determined by measurement of the propagation distance through the waveguide as a function of pulse delay. The squares and solid circles represent measurements at wavelengths 612 nm and 675 nm respectively. The straight lines are linear fits through the data. The group velocity found at $\lambda = 612$ nm is $c/(2.0 \pm 0.6)$. For the red-shifted pulse at 675 nm, the group velocity is $c/(3.4 \pm 0.4)$.

By evaluating the probe position as a function of the arrival time, we readily obtain the group velocity of the pulse propagating in the waveguide. Since we are specifically interested in the even TE mode, the light coupled into the waveguide is selected to be purely TE-polarized.

The relative arrival time of the signal pulse is plotted in Fig. 4 as a function of the propagation distance through the waveguide. We observe a linear dependence of the propagation distance on the pulse delay, with the slope corresponding to the group velocity. The straight line deviations in Fig. 4 and hence the error in group velocity is mainly due to the signal decay along the waveguide and the width of the cross-correlation function (500 – 600 fs). (The cross-correlate is slightly symmetrically broadened due to the non-equal group velocity dispersion in the signal and reference branch [19].) The measurement is performed at the wavelengths 612 nm ($\omega=0.479$) and 675 nm ($\omega=0.434$). For $\lambda = 612$ nm we find a group velocity of $c/(2.0 \pm 0.6)$. The slope of the theoretical dispersion curve suggests a group velocity of $c/2.5$. For $\lambda = 675$ nm, the group velocity is determined to be reduced to $c/(3.4 \pm 0.4)$. The theoretical dispersion curve just starts to flatten off at this wavelength. A quantitative comparison is complicated by the 97% frequency match and limited amount of wavevectors of the FDTD simulation. From the presented data, we derive that the group velocity is reduced to a range between $c/2.7$ and $c/4.6$, which is confirmed by the measurement.

The comparison of both measurements clearly indicates that the group velocity of the TE mode at 612 nm exceeds the value at 675 nm. Since the pulse with the lowest frequency is also the slowest, the dispersion is anomalous [22]. In fact, anomalous dispersion ($d^2k/d\omega^2 < 0$) is typical for the propagation of the even TE mode in W1 PhCWs, in contrast to normal dispersion in conventional index guided waveguides. The anomalous dispersion is also observed as the flattening of the waveguide mode around $\omega = 0.42$ in the theoretical dispersion relation. Hence also the group velocity dispersion shows good correspondence between theory and direct measurement.

5. Conclusion

In conclusion, we have directly measured the local dispersion relation of a PhCW throughout the first two Brillouin zones by employing a phase-sensitive near-field microscope. Fourier transformation of the measured complex field yielded both the amplitude and wavevectors of the modes present in the structure. With this novel approach, we found both positive and negative phase velocities, though only positive group velocities were observed. In the experimental dispersion relation, three waveguide modes are distinguished: two defect guided TE-polarized modes and an index guided TM mode. In the experimental band diagram, two wavevectors were found corresponding to the same TE mode: a direct proof of the propagation of optical Bloch waves, having spatial harmonics in every Brillouin zone. The observed TM-mode however, did show a much weaker Bloch wave behavior. This is attributed to a smaller effective index modulation of the TM mode compared to the TE mode. Group velocity dispersion was addressed by measuring two group velocities of the TE mode. The slower propagating red-shifted pulse demonstrates the anomalous dispersion as is confirmed by the calculations, a conclusion which could not be drawn solely by judging the experimental dispersion relation. Both the measured band diagram and the group velocity measurements are in good agreement with 3D FDTD simulations.